CHEMPHYSCHEM

DOI: 10.1002/cphc.200500307

Spectroscopy and Femtosecond Dynamics of Type-II CdTe/CdSe Core–Shell Quantum Dots

Pi-Tai Chou,*[a] Chun-Yen Chen,[a] Chiu-Ting Cheng,[a] Shih-Chieh Pu,[a] Kun-Chan Wu,[a] Yi-Ming Cheng,[a] Chih-Wei Lai,[a] Yi-Hsuan Chou,[b] and Hsin-Tien Chiu*[b]

Syntheses of CdTe/CdSe type-II quantum dots (QDs) using CdO and $CdCl_2$ as precursors for core and shell, respectively, are reported. Characterization was made via near-IR interband emission, transmission electron microscopy (TEM), energy dispersive spectroscopy (EDX), and X-ray diffraction (XRD). Femtosecond fluorescence upconversion measurements on the relaxation dynamics of the CdTe core (in CdTe/CdSe) emission and CdTe/CdSe interband emission reveal that as the size of the core increases from 5.3, 6.1 to 6.9 nm, the rate of photoinduced electron separation decreases from 1.96, 1.44 to 1.07 $\times 10^{12}$ s^{-1}. The finite rates of the initial charge separation are tentatively rationalized by the small electron–phonon coupling, causing weak coupling between the initial and charge-separated states.

Introduction

Despite well-documented studies of type-I core–shell quantum dots (QDs),[1–7] studies of type-II QDs are relatively rare. Type-II QDs have both valence and conduction bands in the core that are lower (or higher) than those in the shell materials. After electronic excitation, one carrier is predominantly confined to the core, while the other is located in the shell. This spatial separation of charge carriers leads to several characteristic differences from the type-I QDs. On one hand, the interband emission is allowable with an energy gap that would be otherwise inaccessible with type-I structures, extending the color-tuning capability. On the other hand, the spatially separated charges make type-II QDs suitable for photovoltaic applications, in which QDs may replace organic dye chromophores so that one of the photocarriers is injected from the QDs into a matrix prior to the electron/hole recombination.

Recently, based on a colloidal template, a seminal work on the chemical syntheses of type-II CdSe/ZnTe (core/shell) and CdTe/CdSe (core/shell) QDs using $Cd(CH_3)_2$ as a Cd precursor has been reported.[8] This colloidal template approach is crucial in that it provides both feasibility and versatility toward further chemical modification. Subsequently, we have reported the synthesis of CdSe/ZnTe (core/shell) type-II QDs via a safer precursor (CdO) and studied their corresponding excited-state relaxation dynamics.[9] Very recently, a synthetic route to prepare CdTe/CdSe colloidal using a template without incorporating fatty acid, amines, or phosphine oxide was reported.[10] In another approach, interconversion between type-I and II QDs has been achieved via fixing the ZnSe core radius, while increasing the shell (CdSe) thickness.[11] In terms of applications, type-II QDs have been exploited successfully as near-infrared (NIR) dyes for biomedical imaging in living tissue by taking advantage of their great photostability and deeper light penetration.[12]

Note that, in the case of CdSe/ZnTe QDs, both the valence and the conduction bands in the core are lower than those in the shell. Electrons in CdSe being excited cannot circumvent the highly endergonic ZnTe conduction band. Thus, after hole migration the interband emission mainly originates from the CdSe (core) → ZnTe (shell) transition, limiting its application in photovoltaic devices. Alternatively, other type-II QDs, for example, CdTe/CdSe, in which both the valence and conduction bands in the core are higher than those in the shell materials, should be of great interest. Upon excitation, electron injection is likely to be from the conduction band of the shell (i.e. CdSe), providing a driving force to the electron acceptor, for example, TiO_2, commonly used in dye-sensitized solar energy cells. Moreover, the early relaxation dynamics of the core, which may be dominated by electron transfer to the shell, should be different from those of CdSe/ZnTe driven initially by hole transfer to the shell. It is thus important to gain detailed insight into the associated excited-state relaxation dynamics for CdTe/CdSe type-II QDs. In this study, we report the synthesis of CdTe/CdSe type-II quantum dots using safer CdO and $CdCl_2$ as precursors for preparing the core and shell, respectively. Subsequently, absorption, emission and femtosecond time-resolved measurements were carried out for both core (in CdTe/CdSe) emission and CdTe/CdSe interband emission.

[a] *Prof. P.-T. Chou, C.-Y. Chen, C.-T. Cheng, S.-C. Pu, K.-C. Wu, Y.-M. Cheng, C.-W. Lai*
Department of Chemistry, National Taiwan University, Taipei 106 (Taiwan)
Fax: (+886)2-2364-3876
E-mail: chop@ntu.edu.tw

[b] *Y.-H. Chou, Dr. H.-T. Chiu*
Department of Applied Chemistry, National Chiao Tung University
Hsinchu 300 (Taiwan)
E-mail: htchiu@cc.nctu.edu.tw

Results and Discussion

Figure 1 depicts transmission electron microscopy (TEM) images of CdTe core and CdTe/CdSe core/shell type-II QDs. The corresponding composition was characterized by energy dispersive spectroscopy (EDX). As shown in Figure 2a, the appearance of the Se peak at 1.4 keV, in combination with the increase of the ratio for Cd versus Te from 1.2:1 in CdTe to ≈6:1 in CdTe/CdSe, indicates the formation of CdSe. As shown in Figure 2b, comparing the X-ray diffraction (XRD) pattern of the CdTe core, two sets of peaks at faces [100], [002], [101] and [110], [103], [112] shift to higher scattering angle upon coating with the CdSe shell, the results of which are consistent with those reported by Yu et al.[10] In addition, alloy, if it formed, should be supported by a narrowing full-width-at-half-maximum (FWHM) in the set of peaks at [100], [002] and [101]. In contrast, a slight increase of the FWHM was observed upon encapsulating CdSe, supporting the suggestion of the formation of a CdTe/CdSe core/shell structure.

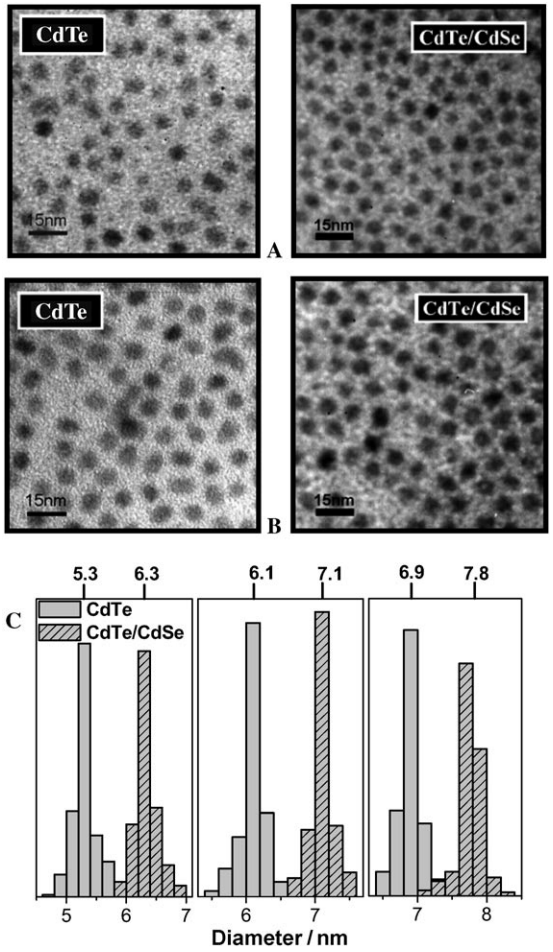

Figure 1. TEM images of the samples with an average of: A) 5.3 nm diameter CdTe QDs (left) and 6.3 nm CdTe/CdSe QDs (right), B) 6.1-nm diameter CdTe QDs (left) and 7.1 nm CdTe/CdSe QDs (right), and C) size histograms for the series of samples described in text. Note that the longest dimension for over 500 particles in each sample has been measured to build the histograms.

To gain a more detailed insight into the composition information we have invested further effort in performing XPS analyses. The peak intensity ratio for elements of the core versus shell as a function of the electron takeoff angle may serve as a valuable tool to extract geometrical information about the nanoparticles.[13] Note that, if QDs were composed of an alloy, the relative peak intensities for Se versus Te would be independent of the electron takeoff angle. Furthermore, empirically, the ratio of the peak area for Te ($3d_{5/2}$) versus Se (3d) is estimated to be 6.82 and 6.68 for X-ray sources at 90° and 54.7°, respectively.[14] Thus, upon normalizing the Se peak intensity, the peak intensity ratio for Te (90°): Te (54.7°) is deduced to be 1.02 for the case of a single layer. Figure 3 shows the XPS spectra of Se and Te peaks for the synthesized CdTe/CdSe QDs at incident angles of 90° and 54.7°, in which the Se peak intensity has been normalized. Accordingly, the intensity ratio for Te (90°):Te (54.7°) was calculated to be 1.26, which is greater than the value of 1.02 deduced from a single layer, that is, an alloy structure. Note that this derivation is based on the empirical data of bulk properties. Thus, the suitability for a similar approach toward nanoscale QDs may not be justified; for example, recently, Piyakis et al.[15] have reported the XPS analysis of spherical Cu nanoclusters. Using angle-resolved XPS, in combination with Monte Carlo simulation, they concluded that, if the radius of the particle is larger than the attenuation length of the photoelectron, the angle dependence may lack good correlation. Nevertheless, the results of angle-dependent XPS, in a qualitative manner, support the formation of CdTe/CdSe core/shell structure. More evidence of a type-II CdTe/CdSe core/shell structure is provided in the section of luminescence studies.

The average sizes of both core-only CdTe and CdTe/CdSe QDs can be estimated directly from TEM (see Figure 1C for size histograms). Unfortunately, the mismatch of the lattice constants between CdTe (6.48 Å) and CdSe (6.05 Å)[16] is only 7.1%, which is too small to allow the resolution of the core and shell individually via the difference in the lattice orientations using TEM. Since the CdTe/CdSe QDs were prepared from the same batch of the CdTe precursor, it is reasonable to assume the same core size in the CdTe/CdSe as in the core-only CdTe. Thus, as an indirect approach, the shell thickness can be estimated by the subtraction of the core size from that of the core/shell particles prepared.

Figure 4 shows the absorption and emission spectra of the CdTe cores and the corresponding CdTe/CdSe QDs, in which the core (core/shell) sizes, measured by TEM size histograms, were calculated to be 5.3 (6.3), 6.1 (7.1) and 6.9 (7.8) nm (see Figure 1). Accordingly, the CdSe thicknesses of these three samples were derived to be 1.0, 1.0 and 0.9 nm, which, within experimental uncertainty, could be treated as constant values. Considering that TEM generally provides insufficient contrast at the edges of nanoparticles, the measured sizes are subject to ≈10% uncertainty on average. Similarly to the CdTe core emission, the NIR interband emission band for CdTe/CdSe QDs also revealed size dependency. Theoretically, the energy gap of the interband emission should correlate with the band offsets of the materials composing the core and the shell. If the shell thickness remains unchanged, the interband exciton emission

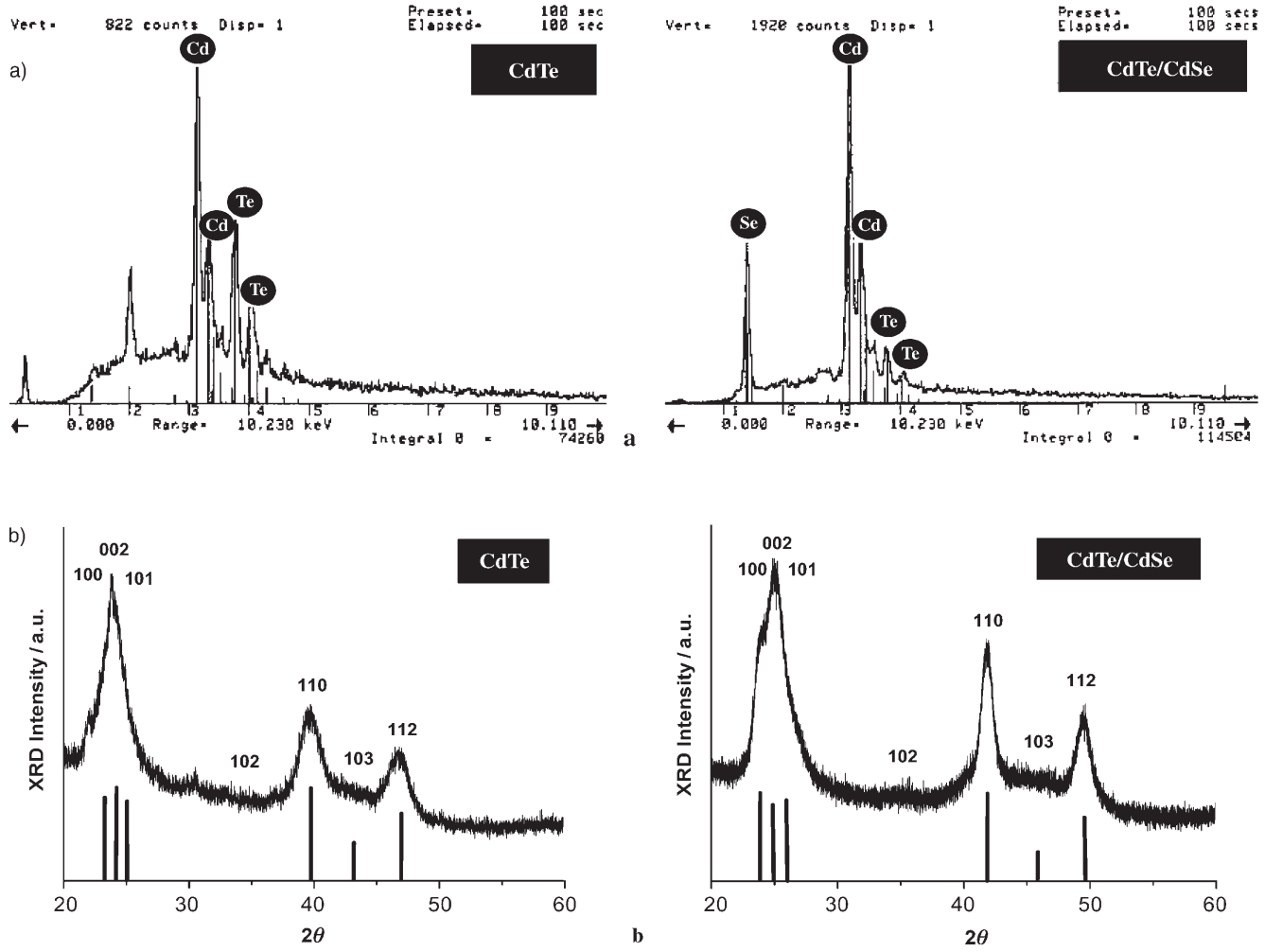

Figure 2. a) Energy dispersive spectroscopy (EDX) characterization of CdTe core (left) and CdTe/CdSe core–shell (right) nanocrystals prepared from $CdCl_2$ precursor described in the text. b) X-ray diffraction (XRD) data on CdTe cores (left) and CdTe/CdSe core/shell nanocrystals (right).

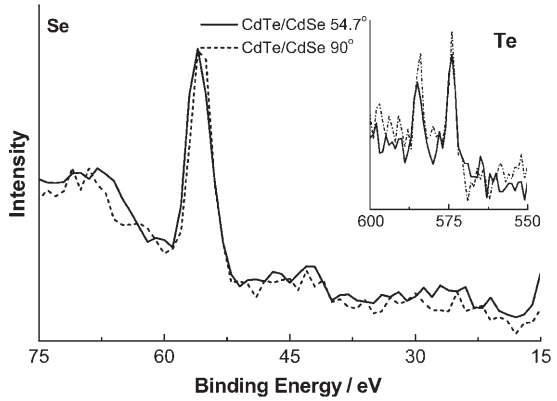

Figure 3. Normalized Se 3d XPS spectra of CdTe/CdSe acquired at electron takeoff angles of 90° (-----) and 54.7° (——). Inset: peak intensity for Te $3d_{5/2}$ at 90° (-----) and 54.7° (—) after normalization with the Se peak.

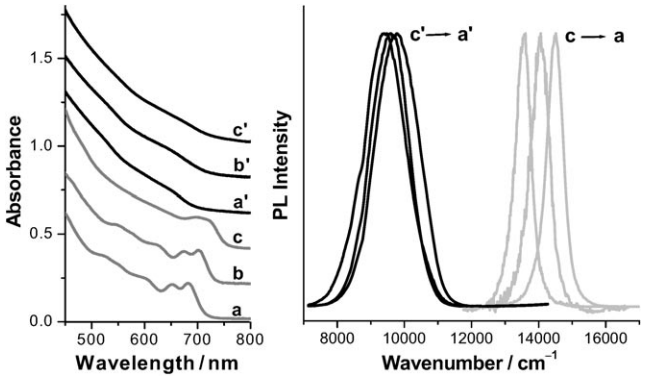

Figure 4. Absorption (left) and emission (right) spectra of CdTe core and CdTe/CdSe core–shell type-II QDs in toluene with different sizes: a) 5.3 nm (core), a′) 6.3 nm (core–shell), b) 6.1 nm (core), b′) 7.1 nm (core–shell), c) 6.9 nm (core), c′) 7.8 nm (core–shell). The average thickness of the shell was estimated to be $\approx 1.0 \pm 0.2$ nm. Note that the x axis in the emission spectrum is in wavenumbers (cm^{-1}) to show the real energy gap.

should be dependent on the size of the core. This is clearly demonstrated in Figure 4. Upon the increase in the diameter of the CdTe cores from 5.3 to 6.9 nm, as indicated by the shift of the CdTe emission peak wavelength from 690 nm (14493 cm^{-1}) to 737 nm (13569 cm^{-1}), the emission of CdTe/CdSe, coated with a similar thickness (1.0 nm) of shell materials (CdSe), shows a systematically bathochromic shift from

1025 nm (9756 cm^{-1}, core 5.3 nm/shell 1.0 nm) to 1061 nm (9425 cm^{-1}, core 6.9 nm/shell 0.9 nm). The results can be rationalized by considering an increased CdTe valence band, that is, a decreasing oxidation potential,[17] upon increasing CdTe size, resulting in a smaller band gap between the CdSe (higher band) and CdTe (lower band). Furthermore, the red shift in pure-core CdTe is 114 meV because of the change in size (from 690 to 737 nm), while the shift in the core/shell CdTe/CdSe QDs, assuming the same shell thickness, is 42 meV (from 1025 to 1061 nm), which is consistent with the model in that the recombination occurs from the CdSe conduction band to the CdTe valence band (type-II). By changing the size of the CdTe core only, the shift in interband emission must be smaller than that for the emission within pure CdTe. We also carefully examined any possible emission band associated with alloy (such as $CdTe_xSe_{1-x}$), the peak wavelength of which is expected to be between that of the CdTe core and the CdTe/CdSe interband emission.[18] The lack of emission originating from alloy firmly supports the CdTe/CdSe core/shell formation.

Table 1 lists room-temperature photophysical properties for CdTe of various sizes and the corresponding CdTe/CdSe QDs. The average population decay times for the core-only CdTe and CdTe/CdSe QDs are in the range of 20–40 ns and 45–60 ns, respectively. In contrast to the strong visible emission of the core ($\Phi_f > 0.1$, see Table 1), the NIR interband emission from CdTe/CdSe QDs is relatively weak. Through a comparison of the emission intensity with that of *meso*-tetraphenylporphyrin ($\Phi_f \approx 0.11$, $\lambda_{max} \approx 760$ nm) in toluene,[19] the quantum efficiency of the NIR interband emission was determined to be of the order of 10^{-1}–10^{-2} (see Table 1). For both CdTe and CdTe/CdSe QDs the emission quantum yields (QYs) increased as the size of the core increased. This tendency might be rationalized, in part, by the formation of crystal defects, which then trap the exciton. Upon decreasing the core size, the surface-to-volume ratio becomes larger, and hence more defects may be developed. For the case of CdTe/CdSe QDs, the radiative decay rate was calculated to be in the range of 10^5–10^6 s^{-1}, which is smaller than that of the core-only CdTe QDs (10^7–10^8 s^{-1}) by approximately two orders of magnitude, on average. The rather long radiative lifetime in CdTe/CdSe may be rationalized by the slow, spatially separated electron–hole recombination of the excitons in type-II structures. Nevertheless, in comparison to the radiative decay rates of 10^4–10^5 s^{-1} for the other type-II QDs such as CdSe/ZnTe,[9] the 10–100-fold increases of the radiative decay rate in CdTe/CdSe would allow us to probe the early relaxation dynamics of the interband emission, which are otherwise inaccessible for CdSe/ZnTe, via the femtosecond fluorescence upconversion approach.[9]

Femtosecond fluorescence upconversion was performed to gain insights into the dynamics of the photoinduced charge separation in the early stage. To elaborate the correlation clearly, we monitored the upconverted emission signal for both core (in CdTe/CdSe) and interband emission. The signal in the region of 650–740 nm, which is ascribed to the precursor core emission, is negligibly small in the steady-state intensity for the CdTe/CdSe QDs due to the dominant charge-separation process. Nevertheless, the upconverted fluorescence signal is relatively much higher than that of the interband emission due to its larger radiative decay rate. Figure 5 reveals the decay dynamics for CdTe/CdSe QDs of various sizes monitored at the peak wavelength of the corresponding core CdTe QDs. It turned out that the temporal trace could be well fitted qualitatively by the convolution of pump–probe cross correlation with a FWHM of $\approx$260 fs in combination with an impulse response $I(t)$ expressed in Equation (1):

$$I(t) = A + Be^{-t/\tau_1} + Ce^{-t/\tau_2} + De^{-t/\tau_3} \quad (1)$$

Three single-exponential components consist of: 1) an ultrafast rise component (τ_1), of which the rise time, within the experimental error, can be barely fitted to be $\approx$160–280 fs; 2) a very fast decay component (τ_2), of which the decay time, depending on the core size, was fitted to be several hundred femtoseconds to $\approx$1 ps; and 3) a very long decay component (τ_3), with a very small, probably negligible, amplitude that can be treated as a constant throughout the measured range of 15 ps. Component (3) was further resolved to be $\approx$45–60 ns via a time-correlated single-photon counting experiment. Table 1 lists the fitted parameters (τ_1 and τ_2) for those CdTe/CdSe QDs studied.

Table 1. Room-temperature photophysical properties for various sizes of CdTe and corresponding CdTe/CdSe QDs in toluene (PL = photoluminescence, QY = quantum yield).

CdTe				CdTe/CdSe						
Size [nm]	PL [nm]	τ[a] [ns]	QY [%]	Size[b] [nm]	PL [nm]	τ_1[c] [fs]	τ_2[c] [fs]	τ_a[d] [fs]	τ_b[e] [ns]	QY [%]
5.3	690 (14993)[f]	21	12	6.3	1025 (9756)[f]	150 ± 60 (−0.49)	510 ± 50 (0.51)	710 ± 50 (−0.50)	45 (0.50)	3.1 ± 0.3
6.1	712 (14045)[f]	36	15	7.1	1043 (9588)[f]	220 ± 60 (−0.48)	690 ± 55 (0.51)	920 ± 70 (−0.50)	48 (0.50)	4.0 ± 0.4
6.9	737 (13569)[f]	34	18	7.8	1061 (9425)[f]	280 ± 70 (−0.49)	930 ± 50 (0.50)	1350 ± 70 (−0.50)	55 (0.50)	5.2 ± 0.2

[a] The average decay time at room temperature. [b] The core–shell size was synthesized from its corresponding core, and the average shell thickness was $\approx$1.0 nm. [c] The rise and decay components [see Eq. (1)] measured at peak wavelength supposed for the core emission. [d] τ_a: the rise time of the interband emission. [e] τ_b: the population decay component of the interband emission was obtained from the time-correlated single-photon-counting measurement. [f] The units are in wavenumbers (cm^{-1}). Numbers in parentheses of [c]–[d] are the normalized pre-exponential values. Note that the pre-exponential value of τ_b was taken from the upconverted signal.

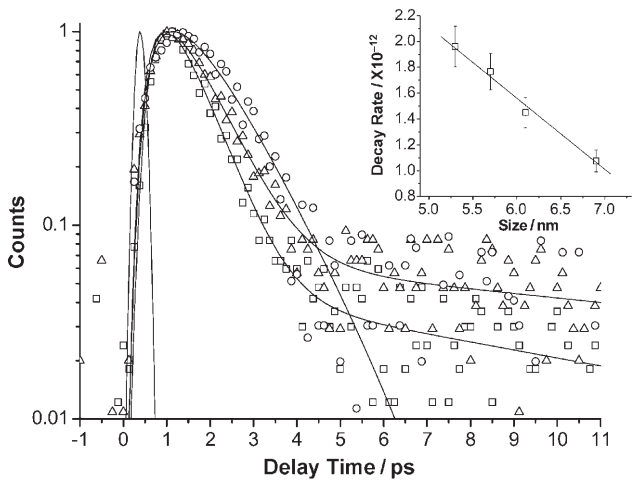

Figure 5. The fluorescence upconversion signal for CdTe/CdSe QDs in toluene with a core diameter of 5.3 nm (□), 6.1 nm (△) and 6.9 nm (○). Emission is monitored at the peak wavelength of the corresponding core, i.e., 690, 712 and 737 nm, respectively. (——) system response function. Insert: The plot of electron separation rate as a function of the core diameter. Note that an additional point of core (5.7 nm)/shell (1.0 nm) is added in the plot. The average thickness of shell (CdSe) is ≈1.0 nm for all QDs. λ_{ex}: 400 nm.

As for component (3), because the available excitation wavelength was tuned to 380–420 nm in the fluorescence upconversion study, it is possible that direct excitation of the CdSe shell was also possible.[20,21] Support of this viewpoint was given by both steady-state and nanosecond time-correlated single-photon counting measurements, in which a weak emission with the peak wavelength of ≈550 nm (τ_f ≈13 ns, not shown here) was resolved upon excitation at <400 nm. In comparison, the 550-nm band was absent in the CdTe core-only QDs. However, for type-II CdTe/CdSe QDs, photoexcitation of the shell CdSe should result in a very rapid electron transfer due to the same charge-separated state as the core excitation. It is thus more plausible to attribute the very-weak-intensity long-decay component to a trace concentration of freestanding CdSe particles generated from nucleation during the shell growth. Nevertheless, due to its small amplitude and long population decay, this component is simply neglected in the following discussion.

As to the fast decay component (2), when the size of the CdTe core increased to 5.3, 6.1 and 6.9 nm, the lifetime of the decay component (2) systematically increased to 510±50 fs, 690±55 fs and 930±50 fs, respectively. Assuming that the fast quenching of the core emission in CdTe/CdSe is dominated by the rate of photoinduced electron transfer to the shell, the plot for the rate of interfacial electron transfer versus the core diameter reveals a straight-line-like correlation (see the insert of Figure 5). The result seems to be different from a convex-curve-like plot for the CdSe/ZnTe type-II QDs.[9] This discrepancy may simply reflect the material difference between these two types of QDs. However, it should be noted that the plot for CdSe/ZnTe QDs is based on a large variation (≈1.8 fold) of core sizes, ranging from 3.0 to 5.5 nm, while the largest difference in the core size could be prepared is 1.6 nm (5.3–6.9 nm, ≈1.3 fold) for the CdTe/CdSe QDs. Thus, unless a wider range of CdTe core sizes can be obtained, a fair comparison of charge-separation rates between CdTe/CdSe and CdSe/ZnTe QDs may not be meaningful at this stage.

Finally, although the time scale of the rise component (1) is within the borders of the detection response limit, it can still be barely resolved and appears to increase as the core size increases from 5.3 nm (150±60 fs) to 6.9 nm (280±70 fs). Since the excitation wavelengths of 380–410 nm are well above the lowest-lying conduction band of the CdTe core, we tentatively propose that the finite rise component may originate from a fast internal conversion, followed by a relaxation to the lowest conduction band. However, due to its nearly detection-response-limited time scale, we believe that any quantitative attempts to ascertain the corresponding mechanism will be based on too much speculation and hence may not be reliable.

Attempts to acquire the femtosecond upconverted signal of the interband emission for the CdTe/CdSe QDs with various core sizes were also made. The time-dependent trace is shown in Figure 6, while corresponding data are listed in Table 1. In all

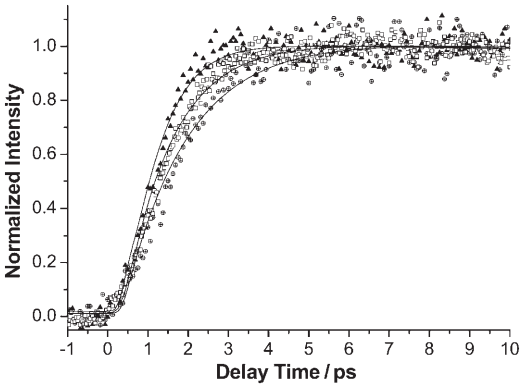

Figure 6. The fluorescence upconversion signal for CdTe/CdSe QDs in toluene with a core diameter of 5.3 nm (▲), 6.1 nm (□) and 6.9 nm (⊕). Emission is monitored at the peak wavelength of the interband emission, i.e., 1025, 1043 and 1061 nm, respectively. (——): the corresponding fitting curves (see text). The average thickness of shell (CdSe) is ≈1.0 nm for all QDs. λ_{ex}: 400 nm.

cases, the experimental results could be best fitted by the convolution of pump-probe cross correlation with a FWHM of ≈180 fs in combination with the impulse response $I(t)$ consisting of a resolvable rise (negative pre-exponential value) exponential component and a nearly constant value throughout the acquisition time of 10 ps. It should be noted that fitting the data using only the cross correlation plus a constant value gave a worse fit, in particular because the initial fluorescence intensity could not be fully simulated. The constant value within 10 ps simply indicates a much longer decay time, which has been further resolved to be around several tens of nanosecond via the nanosecond time-correlated single-photon counting experiment (see Table 1).

Before further discussing the observed relaxation dynamics, a brief review of femtosecond approaches in the light of other works on II–VI QDs seems necessary, although most researches

focus on the CdSe type-I QDs. For the case of CdSe, both electron and hole relaxation pathways have been studied extensively via either transient absorption[22–25] or fluorescence upconversion techniques.[26–27] Most ultrafast measurements display multi- exponential dynamics, consisting of rise times of less than a few picoseconds for the population of the excited state, followed by 1–10 ps decay components and a nanosecond or even longer population lifetime. On the basis of a full-range, that is, visible/near-IR/IR, transient absorption technique, Burda et al.[25] were able to resolve the relaxation dynamics ascribed to the electron and hole separately. It is now commonly accepted that the population of the conduction-band edge by the electron occurs within several hundred femtoseconds, whereas the whole relaxation—at least for the case of CdSe QDs—is relatively slow ($\approx$1–10 ps).[25] Accordingly, the hole relaxation seems to be rate limiting in the intraband relaxation process of the excited CdSe QDs. As for the mechanism of the relaxation dynamics, a majority of reports have argued against the existence of the phonon bottleneck in CdSe QDs, a bulk property which governs the energy relaxation of excitons via electron–phonon coupling in the lattice. Instead, a combination of internal conversion, trapping and Auger-like processes[28,29] seems to play a key role for the observed relaxation dynamics. Nevertheless, one should be aware that differences in the results can be found, depending on the sample characteristics. It has been pointed out that CdSe QDs sample prepared in different research groups revealed different surface properties and hence different relaxation dynamics.[25]

In addition to the aforementioned single-exciton experiments, more recently, exquisite works have been carried out in several research groups to resolve the spectroscopy and dynamics of multiexcitons in CdSe QDs. In a seminal study, Klimov et al.[30] have resolved the relaxation kinetics of two, three and four electron–hole pairs in CdSe QDs using femtosecond transient absorption spectroscopy. Subsequently, by applying a fluorescence upconversion technique with a method of spectra temporal evolution, several groups were able to resolve the transient emission ascribed to neutral, charged biexcitons and neutral triexciton under high-power excitation.[31–33] For comparison, herein, the 400-nm femtosecond pulse was reduced to less than 10 mW (80 or 4 MHz), and the density of energy per pulse was calculated to be less than 1.6×10^{-8} J cm^{-2}, which is equivalent to a photon flux of less than 3.2×10^{10} photon cm^{-2}. Thus, laser power has been reduced to ensure that only one exciton was formed per QDs. Under this configuration we believed that the yielding relaxation dynamics should be free from effects such as bi- or multi-exciton annihilation.

Upon monitoring at CdTe (core) emission in CdTe/CdSe QDs, the relaxation dynamics on a time scale of less than one picosecond with the complete disappearance of any long-lived component is drastically different from the much slow 20–40 ns exciton recombination time obtained in core-only CdTe (see Table 1). Furthermore, due to the significant CdTe size dependence, with a slower decay rate as the CdTe core size increases, it is less likely that the sub-picosecond decay can simply be attributed to the internal electron relaxation process. Alternatively, we tentatively attribute the fast CdTe relaxation dynamics in type-II CdTe/CdSe QDs to a very rapid electron transfer from CdTe (core) to CdSe (shell), as shown in the cover picture. Further support can be provided from the correlation of the dynamic data. As shown in Table 1, the rise component of the interband emission increases as the core size increases. For example, the rise component increases from 710 ± 50 fs, 920 ± 70 fs to 1350 ± 70 fs as the size of CdTe in CdTe/CdSe QDs increases from 5.3, 6.1 to 6.9 nm. The results, within experimental uncertainty, correlate well with the decay components of the CdTe core (in CdTe/CdSe) emission, and can thus be rationalized by a precursor–successor type of charge separation from the CdTe (core) valence band to the CdSe (shell) conduction band upon electronic excitation. For interband emission the tendency for slightly longer rise component than the decay time monitored on core emission indirectly supports the finite internal conversion rate prior to charge separation. Apparently, both the decay for core emission and the rise dynamics for the interband emission are consistent, which reveals that, as the size of the core increases, the rate of charge separation decreases. One plausible mechanism lies in the fact that the finite rate of charge separation may be due to the low electron–phonon coupling.[34] Increasing the core size causes a drop in the CdTe conduction band.[35] As a result, the energy gap between the CdTe and CdSe conduction bands is smaller, so that the density of electron–phonon coupling may be reduced, resulting in the decrease in the charge-separation rates. Nevertheless, further theoretical effort is necessary to shed light on the corresponding fundamentals.

Conclusions

In summary, we have synthesized CdTe/CdSe QDs from the much safer CdO and $CdCl_2$ precursors for core and shell, respectively, to perform spectroscopy and investigate the dynamics of the type-II interband emission. Based on the femtosecond upconversion technique, we report on the first observation of early relaxation dynamics on CdTe/CdSe type-II QDs interband emission. The results indicate that the electron-separation rate decreases as the size of the cores increases. Due to the absence of observation of coherent optical phonon modes for both CdTe core (in CdTe/CdSe) emission and CdTe/CdSe interband emission, it is possible that the finite rate of charge separation is due to the small electron–phonon coupling, causing weak coupling between the initial and charge-separated states. We believed that the results shown here, especially the degree of control of the rate of electron transfer, may be crucial in applications where rapid carrier separation followed by charge transfer into a matrix or electrode is important, as in photovoltaic devices.

Experimental Section

Tri-*n*-octylphosphine oxide (TOPO, 99%, Aldrich), tri-*n*-butylphosphine (TBP, technical grade 98%, SHOWA), tri-*n*-octylphosphine (TOP, TCI), hexadecylamine (HDA, 90%, TCI), CdO (99.99%, Strem), $CdCl_2$ (99.99%, Aldrich), selenium (Se) powder 200 mesh (99.5%,

Aldrich) and Tellurium (Te) powder 200 mesh (99.8%, Aldrich) were used immediately on receipt.

The preparation of the CdTe core from CdO was according to a method previously reported by Peng and coworkers.[36] To obtain the CdTe/CdSe core/shell nanoparticles, the precipitated CdTe QDs (0.020 g) were dispersed in TOPO (2.20 g) and HDA (1.26 g) before being heated to 190 °C. In addition, $CdCl_2$ (0.092 g) was dissolved in TBP (2.5 mL) upon gentle heating (ca. 80 °C). After being cooled to room temperature, the resulting 0.2 M solution was mixed with Se (2.5 mL, 0.2 M in TBP). With a syringe pump, this mixture was injected within 1 h into the reaction flask containing the core nanocrystals at 190–200 °C. After the addition was completed, the crystals were annealed at 190 °C for an additional 1–1.5 h. Core/shell nanoparticles of various sizes were obtained by adjusting the concentrations of $CdCl_2$ and Se in TBP as well as the corresponding injection periods. The prepared CdTe/CdSe QDs were further purified by centrifugation and double reprecipitation from methanol.

The sizes of QDs were determined with a Hitachi H-7100 TEM. Further characterization of the QDs was made with powder X-ray diffraction (XRD, model PANalytical X' Pert PRO) and X-ray photoelectron spectroscopy (XPS, model VG Scientific ESCALAB 250). UV/Vis steady-state absorption and emission spectra were recorded with a Hitachi (U-3310) spectrophotometer and an Edinburgh (FS920) fluorimeter, respectively. The type-II NIR emission spectra were obtained by exciting the sample solution under a front-face excitation configuration using an Ar ion laser (488 or 514 nm, Coherent Innova 90). The emission was then sent through an NIR-configured Fourier-transform interferometer (Bruker Equinox 55) and detected with an NIR-sensitive photomutiplier (Hamamatsu model R5509–72) operated at −80 °C. Details of nanosecond lifetimes and femtosecond fluorescence upconversion measurements have been described previously.[9]

Acknowledgements

The authors would like to gratefully acknowledge the financial support from the National Science Foundation, Taiwan and National Taiwan University.

Keywords: colloids · core–shell materials · crystal growth · femtosecond chemistry · semiconductors

[1] A. P. Alivisatos, *Science* **1996**, *271*, 933 – 937.
[2] M. Danek, K. F. Jensen, C. B. Murray, M. G. Bawendi, *Chem. Mater.* **1996**, *8*, 173 – 180.
[3] B. O. Dabbousi, J. Rodriguez-Viejo, F. V. Mikulec, J. R. Heine, H. Mattoussi, R. Ober, K. F. Jensen, M. G. Bawendi, *J. Phys. Chem. B* **1997**, *101*, 9463 – 9475.
[4] Nirmal, L. Brus, *Acc. Chem. Res.* **1999**, *32*, 407 – 414.
[5] H. Mattoussi, J. M. Mauro, E. R. Goodman, G. P. Anderson, V. C. Sundar, F. V. Mikulec, M. G. Bawendi, *J. Am. Chem. Soc.* **2000**, *122*, 12142 – 12150.
[6] D. V. Talapin, A. L. Rogach, A. Kornowski, M. Haase, H. Weller, *Nano Lett.* **2001**, *1*, 207 – 211.
[7] P. Reiss, J. Bleuse, A. Pron, *Nano Lett.* **2002**, *2*, 781 – 784.
[8] S. Kim, B. Fisher, H. J. Eisler, M. G. Bawendi, *J. Am. Chem. Soc.* **2003**, *125*, 11466 – 11467.
[9] C. Y. Chen, C. T. Cheng, J. K. Yu, S. C. Pu, Y. M. Cheng, P. T. Chou, Y. H. Chou, H. T. Chiu, *J. Phys. Chem. B* **2004**, *108*, 10687 – 10691.
[10] K. Yu, B. Zaman, S. Romanova, D. Wang, J. A. Ripmeester, *Small* **2005**, *1*, 332 – 338.
[11] L. P. Balet, S. A. Ivanov, A. Piryatinski, M. Achermann, V. I. Klimov, *Nano Lett.* **2004**, *4*, 1485 – 1488.
[12] S. Kim, Y. T. Lim, E. G. Soltesz, A. M. De Grand, J. Lee, A. Nakayama, J. A. Parker, T. Mihaljevic, R. G. Laurence, D. M. Dor, L. H. Cohn, M. G. Bawendi, J. V. Frangioni, *Nat. Biotechnol.* **2004**, *22*, 93 – 97.
[13] I. Tunc, S. Suzer, M. A. Correa-Duarte, L. M. Liz-Marzan, *J. Phys. Chem. B* **2005**, *109*, 7597 – 7600.
[14] C. D. Wagner, L. E. Davis, M. V. Zeller, J. A. Taylor, R. H. Raymond, L. H. Gale, *Surf. Interface Anal.* **1981**, *3*, 211 – 225.
[15] K. N. Piyakis, D.-Q. Yang, E. Sacher, *Surf. Sci.* **2003**, *536*, 139 – 144.
[16] S. M. Sze, *Physics of Semiconductor Device*, New York, Wiley Interscience Publication, **1981**, p. 848 – 849.
[17] E. Kucur, J. Riegler, G. A. Urban, T. Nann, *J. Chem. Phys.* **2003**, *119*, 2333 – 2337.
[18] R. E. Bailey, S. Nie, *J. Am. Chem. Soc.* **2003**, *125*, 7100 – 7106.
[19] P. G. Seybold, M. Gouterman, *J. Mol. Spectrosc.* **1969**, *31*, 1 – 13.
[20] E. H. Lee, S. Stoltz, H. C. Chang, M. H. Na, H. Luo, A. Petrou, *Solid State Commun.* **1998**, *107*, 177 – 181.
[21] J. Haetty, E. H. Lee, H. Luo, A. Petrou, J. Warnock, *Solid State Commun.* **1998**, *108*, 205 – 208.
[22] V. I. Klimov, D. W. McBranch, *Phys. Rev. Lett.* **1998**, *80*, 4028 – 4031.
[23] V. I. Klimov, D. W. McBranch, C. A. Leatherdale, M. G. Bawendi, *Phys. Rev. B* **1999**, *60*, 13740 – 13749.
[24] V. I. Klimov, Ch. J. Schwarz, D. W. McBranch, C. A. Leatherdale, M. G. Bawendi, *Phys. Rev. B* **1999**, *60*, R2177-R2180.
[25] C. Burda, S. Link, M. Mohamed, M. A. El-Sayed, *J. Phys. Chem. B* **2001**, *105*, 12286 – 12292.
[26] V. Klimov, P. Haring Bolivar, H. Kurz, *Phys. Rev. B* **1996**, *53*, 1463 – 1467.
[27] D. F. Underwood, T. Kippeny, S. J. Rosenthal, *J. Phys. Chem. B* **2001**, *105*, 436 – 443.
[28] A. L. Efors, V. A. Kharchenko, M. Rosen, *Solid State Coummun.* **1995**, *93*, 281 – 284.
[29] S. Xu, A. A. Mikhailovsky, J. A. Hollingsworth, V. I. Klimov, *Phys. Rev. B* **2002**, *65*, 045 319.
[30] V. I. Klimov, A. A. Mikhailovsky, D. W. McBranch, C. A. Leatherdale, M. G. Bawendi, *Science* **2000**, *287*, 1011 – 1013.
[31] M. Achermann, J. A. Hollingsworth, V. I. Klimov, *Phys. Rev. B* **2003**, *68*, 245 302.
[32] J.M Caruge, Y. T. Chan, V. Sundar, H. J. Eisler, M. G. Bawendi, *Phys. Rev. B* **2004**, *70*, 085 316.
[33] C. Bonati, M. B. Mohamed, D. Tonti, G. Zgrablic, S. Haacke, F. V. Mourik, M. Chergui, *Phys. Rev. B* **2005**, *71*, 205 317.
[34] H. Benisty, C. M. Sotomayor-Torres, C. Weisbuch, *Phys. Rev. B* **1991**, *44*, 10945 – 10948.
[35] S. K. Haram, B. M. Quinn, A. J. Bard, *J. Am. Chem. Soc.* **2001**, *123*, 8860 – 8861.
[36] Z. A. Peng, X. Peng, *J. Am. Chem. Soc.* **2001**, *123*, 183 – 184.

Received: June 9, 2005
Revised: August 17, 2005

